Applied Radiation and Isotopes 165 (2020) 109221

Contents lists available at ScienceDirect

Applied Radiation and Isotopes

journal homepage: http://www.elsevier.com/locate/apradiso

Determination of eccentric deposition thickness on offshore horizontal pipes by gamma-ray densitometry and artificial intelligence technique

Tâmara P. Teixeira [a,*], Marcelo C. Santos [c], Caroline M. Barbosa [b], William L. Salgado [b], Roos Sophia F. Dam [b], César M. Salgado [b], Roberto Schirru [c], Ricardo T. Lopes [a]

[a] Laboratório de Instrumentação Nuclear (COPPE/UFRJ), P.O Box 68509, Rio de Janeiro, RJ, Brazil
[b] Instituto de Engenharia Nuclear (CNEN/ RJ), P.O Box 68550, Rio de Janeiro, RJ, Brazil
[c] Laboratório de Monitoramento e Processamento (COPPE/UFRJ), Rio de Janeiro, RJ, Brazil

ARTICLE INFO

Keywords:
Barium sulfate scale
MCNPX code
Gamma-ray densitometry
Deep artificial neural network (DNN)
Deep learning

ABSTRACT

The extraction of oil is accompanied by water and sediments that, mixed with the oil, cause the formation of scale depositions in the pipelines walls promoting the reduction of the inner diameter of the pipes, making it difficult for the fluids to pass through interest. In this sense, there is a need to control the formation of these depositions to evaluate preventive and corrective measures regarding the waste management of these materials, as well as the optimization of oil extraction and transport processes. Noninvasive techniques such as gamma transmission and scattering can support the determination of the thickness of these deposits in pipes. This paper presents a novel methodology for prediction of scale with eccentric deposition in pipes used in the offshore oil industry and its approach is based on the principles of gamma densitometry and deep artificial neural networks (DNNs). To determine deposition thicknesses, a detection system has been developed that utilizes a 1 mm narrow beam geometry of collimation aperture comprising a source of ^{137}Cs and three properly positioned 2″×2″ NaI(Tl) detectors around the system, pipe-scale-fluid. Crude oil was considered in the study, as well as eccentric deposits formed by barium sulfate, $BaSO_4$. The theoretical models adopted a static flow regime and were developed using the MCNPX mathematical code and, secondly, used for the training and testing of the developed DNN model, a 7-layers deep rectifier neural network (DRNN). In addition, the hyperparameters of the DRNN were defined using a Baysian optimization method and its performance was validated via 10 experiments based on the K-Fold cross-validation technique. Following the proposed methodology, the DRNN was able to achieve, for the test sets (untrained samples), an average mean absolute error of 0.01734, mean absolute relative error of 0.29803% and R2 Score of 0.9998813 for the scale thickness prediction and an average accuracy of 100% for the scale position prediction. Therefore, the results show that the 7-layers DRNN presents good generalization capacity and is able to predict scale thickness with great precision, regardless of its position inside the tube.

1. Introduction

In the petroleum industry, the study of scale is of great interest regarding pipelines and equipment for the primary processing of fluids such as gas, oil and water. The extraction of petroleum is accompanied by water and sediment, mixed with the oil, form scales in the walls of the pipes causing the reduction of the internal diameter making it difficult to pass the fluid (Martin et al., 1997; Coto et al., 2008; Kan and Thomson, 2012; Yan et al., 2004).

The formation of scale occurs by mixing water containing preferentially dissolved ions when subjected to favorable thermodynamic conditions. Water associated with the oil well (formation water), when mixed with injection water (usually seawater), forms the production water. Due to the chemical affinity of the seawater soluble elements and the formation water, chemical interactions may occur which will favor the formation of inorganic deposits, scales.

In offshore production, the formation of sulfate incrustations is generally common during secondary recovery (water flooding). In order to optimize the production of oil wells, seawater (containing sulfate ions, SO_4^{2-}) is injected into the reservoir, mixing with the cations present in the formation water (Ba^{2+}, Ca^{2+}, Mg^{2+} e Sr^{2+}), and leading to mineral precipitation. This formation, regardless of where it is deposited,

* Corresponding author.
E-mail address: tteixeira@con.ufrj.br (T.P. Teixeira).

https://doi.org/10.1016/j.apradiso.2020.109221
Received 20 December 2019; Received in revised form 7 April 2020; Accepted 4 May 2020
Available online 26 June 2020

prevents runoff, resulting in a reduction in production and also in damage to the equipment. The most common sulfate incrustations found by the oil industry are barium sulfate ($BaSO_4$), strontium sulfate ($SrSO_4$) and calcium sulfate ($CaSO_4$). Barium sulfate ($BaSO_4$) is particularly tough due to its high resistance to chemical and mechanical treatments (Graham et al., 2004; Ferreira, 2011; Bukuaghangin et al., 2016).

Extensive studies aim to characterize and identify scales in oil pipelines to minimize their impacts on oil and gas production. Particularly noteworthy are the deposits of barium sulfate (Bjornstad and Stamatakis, 2006a; Amari and Moghadasi, 2010; Khatami et al., 2010; Oliveira et al., 2015, 2019; Bukuaghangin et al., 2016; Teixeira et al., 2018; Salgado et al., 2019), due to their low solubility in water and consequent higher deposition probability compared to other salts (Godoy, 2003; Araújo, 2005; Ferreira, 2011; Beserra, 2012).

The occurrence of scale is a serious problem in the production process of the oil and gas industry, so there is a need for control and monitoring of scales thicknesses in processes involving the transport of oil to minimize corrective maintenance in these facilities without, however, stopping at the operating plant.

Numerous articles describe methods that involve the study of chemical kinetics to predict the formation of scales. Kinetic methods are based on predicting the saturation index of dissolved sulfates in the production water and monitoring the change in pH, temperature and concentration necessary for the precipitation of mineral scales (Olajire, 2015; Bukuaghangin et al., 2016). On the other hand, non-kinetic methods are based on physical changes in some points of the transport system such as pressure and temperature monitoring, which only indicate the occurrence of the problem at an advanced stage.

However, in the context of non-kinetic/thermodynamic techniques, radioactive techniques are being used to detect depositions in oil pipelines using radiotracers (Bjornstad and Stamatakis, 2006b), neutrons (Abdul-Majid et al., 1989, 1996, 2013), computed radiography and x-ray microfluorescence (Candeias et al., 2014), x-ray microtomography (Oliveira et al., 2019) and gamma ray densitometry (Monno, 1985; Sowerby and Rogers, 2005; Oliveira et al., 2015; Teixeira and Salgado, 2017; Beserra, 2012; Teixeira et al., 2018; Salgado et al., 2019).

The gamma ray densitometry technique, one of the non-destructive testing methods, has been applied and obtained satisfactory results in many areas such as petrochemical, oil industry and mining. It has been used for flow measurement studies (Mi et al., 1998; Salgado et al., 2009, 2010; Roshani et al., 2015, 2017a, 2017b, 2018); for density prediction (Achmad and Hussein, 2004; Roshani et al., 2013; Salgado et al., 2019), for the study of thickness measurements (Berman and Harris, 1954); for the detection of vertical pipe depositions and corrosion in pipelines used for oil extraction (Monno, 1985; Drake and Seward, 1989; Beserra, 2012; Oliveira et al., 2015; Teixeira and Salgado, 2017; Teixeira, 2018; Salgado et al., 2019).

The thickness of the scales, mainly with eccentric formation, are not easy to determine because they present non-uniform deposition inside the pipes, making it difficult to locate and identify the maximum thickness of the deposit in certain points of the pipe. Besides, there is the presence of fluids (gas, water and oil), which directly interfere in the accuracy of the evaluation of the scale thickness, since the gamma-ray attenuation has the Compton scattering and the photoelectric effect as predominant interactions and the transversal sessions for both are proportional to the density of each material.

Among the nuclear techniques, gamma-ray densitometry is based on the transmission of a gamma-ray beam to determine the specific density of the material and your thickness. A radiation detector records the transmitted gamma-ray flux through the pipeline, the scale and the inner fluid. Transmission measurement enables monitoring of the entire oil extraction process without operational interference, and has proven to be a potential solution for the preventive control of scale (Bjørnstad e Stamatakis, 2006a; Oliveira et al., 2015; Teixeira et al., 2018; Salgado et al., 2019). Therefore, it is a non-invasive technique (the detector used in gamma acquisition is installed outside the pipe and is not in contact with the fluids) that can detect and quantify incrustation with a single measurement geometry.

Density calibration can be performed by comparing the counts recorded by the detectors with the actual density. However, the analytical equations are specific to a given geometry and fluid flow regime and it is clear that these parameters should not be significantly changed to obtain reliable results.

In order to get around these problems, Artificial Intelligence (AI) techniques as artificial neural networks (ANNs), especially in their more modern deep learning variants which in the recent years have proven themselves to be one of the most efficient AI methods for patterns recognition problems, can provide subsidies for the determination of scale thicknesses without, however, requiring so much information inside the pipe and other constituents of the same.

The ANNs can be described as mathematical models originally inspired by the functioning of the brain, which can learn from examples, extracting knowledge from the raw data through the patterns present in it (Haykin, 1999). Due to the capacity of the ANNs models of learning the patterns in the data and generalize them, these models have been coupled with techniques that use gamma radiation sources to interpret the Pulse Height Distributions (PHD) obtained by radiation detector for the identification of flow regimes and prediction of volume fractions in multiphase systems (Salgado et al., 2019; Salgado et al., 2010), to predict the density of oil and derivatives (Salgado et al., 2019), to predict the thickness of concentric inorganic scale in oil pipelines (Teixeira and Salgado, 2017; Teixeira et al., 2018; Salgado et al., 2019).

The cited works show that ANNs were able to achieve satisfactory results, proving the feasibility of using this type of approach to solve this class of problem. However, in these applications, relatively small datasets were used, with only about 100 examples, to train and test the ANNs. Besides that, in most part of these works, simple ANN models were used, more specifically shallow neural networks (SNNs) architectures with few internal processing layers. As already shown in the literature (Srivastava et al., 2015), these shallow ANN models tend to present inferior learning and generalization capability than deep learning models, which are deep neural networks (DNNs) architectures with multiple internal processing layers. The superior capacity of deep learning models stands out especially in more complex problems, where a large dataset, with thousands of examples, is necessary to cover the entire search space of the problem (Gheisari et., 2017).

The DNNs have same basic concept as its shallow contra parts, having the ability to learn from examples and to model complex non-linear relationships between these examples. However, the main difference and advantage of the DNNs is that these models have many layers of non-linear parametrized processing units (called hidden layers) separating the input and output layers, while, in contrast, the SNNs have very few hidden layers. Besides, the greater number of layers permits that the DNNs learning process to operate based on the concept of hierarchical learning (more commonly called deep learning), that is more similar to how the visual cortex of the brain works, that is hierarchically (Lewis et., al 2000). Thus, in this learning concept, representations of complex characteristics of a problem are expressed in terms of simpler representations, since each successive layer of an DNN uses the output from the previous layer as input. This approach allows DNNs to be able to deal with extremely complex problems, since the learning happens in multiple levels with the higher and complex level features of the problem being learned derived from previously learned lower and simple level features (Benuwa et al., 2016).

In this context, it is proposed in this study a novel approach that uses a simulated model based on gamma-ray densitometry coupled with a DNN to determine the scale thickness. In this approach, the elaboration of this model and the vast amount of data obtained through the transmission and scattering gamma can be used to train and test a DNN architecture to predict the location and maximum scale thickness.

Monte Carlo eXtensed N-Particle (MCNPX) is a computational tool that simulates the transport of radiation in matter, such as neutrons,

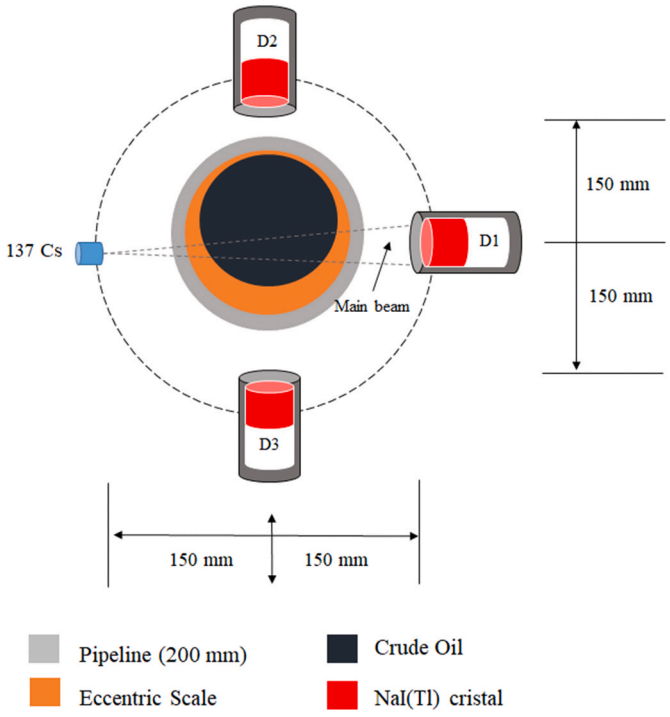

Fig. 1. Representation of the scale measurement model in a horizontal pipe.

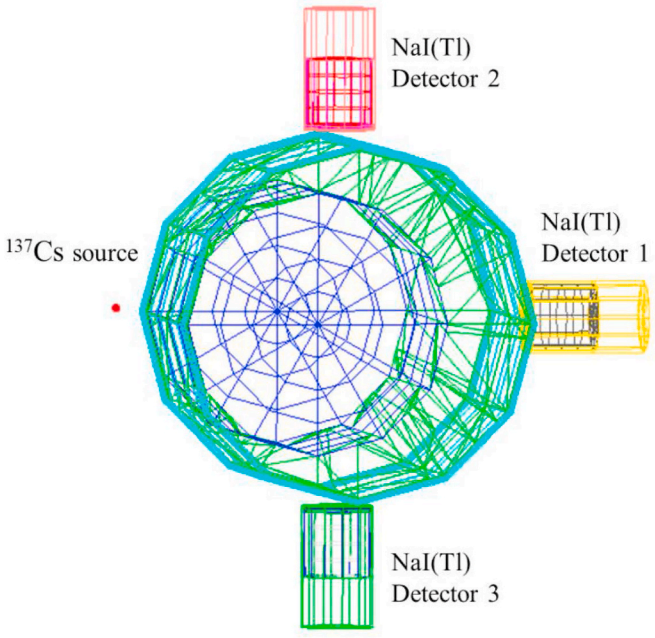

Fig. 2. Scale measurement model in a horizontal pipeline by Moritz 1.12 graphics software.

photons and electrons, and is used in situations where physical measurements are inconvenient, difficult or even impossible.

Gamma ray simulation with MCNPX code includes Rayleigh and Compton scattering, X-ray fluorescence, pair production and bremsstrahlung (Pelowitz, 2005) and thus can be applied in radioprotection studies, nuclear power plants, radiation detector modeling, nuclear applications in industry and so on. The models developed for this study, in the MCNPX code, consider the main effects of radiation interaction with matter and the PHDs of NaI(Tl) detectors.

The scale is analyzed using patterns containing the location/thickness information. PHDs are used to feed (train) the DNN which can learn to classify different thicknesses automatically and thus more accurately predict scale thicknesses of new patterns. The set of patterns (different thickness and scale location) used for training and evaluation of the DNN generalization capacity can be obtained by mathematical simulation using a Monte Carlo computational code (Abro et al., 1999a, 1999b). Due to the difficulties inherent to the choice of experimental data to train the DNN, the radiation simulator based on the Monte Carlo method was used in this study.

2. Methodology

In this study, MCNPX code was used to simulate gamma-rays scattering and transmission from a radiation source in static flow regime in pipeline using three detectors. By the use of MCNPX simulations, it was possible to generate an appropriated data set for training an DNN.

2.1. Detection geometry

The detection system consists of three 50.8 mm × 50.8 mm, (2″ × 2″) NaI(Tl) scintillators detectors (Oliveira et al., 2015; Beserra, 2012) positioned orthogonally in relation to a 662 keV collimated gamma-ray source. The established divergence of the source is 5.73°, corresponding to a collimation opening of 2 mm (Teixeira et al., 2018). A non-analog simulation was used to reduce efforts and computational times, biasing the directions of emission from the source to the detector. Thus, the point source was collimated with a cone configuration using the SI,

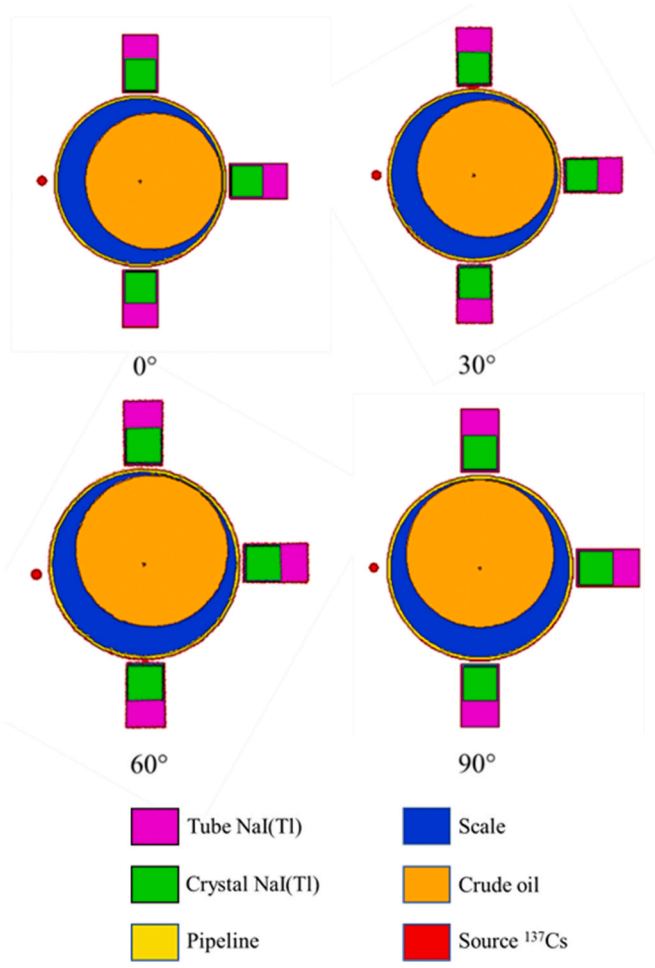

Fig. 3. Scale localizations model in a horizontal pipeline by Vized X22S graphics software.

SP and SB cards available at the MCNPX code. To detect the main beam transmitted, a detector was positioned at 180° from the point source and to detect the scattered beams, the other detectors were positioned, namely at 90° and 270°. The PHDs gamma-ray acquired by the detectors were used directly to feed an ANN. The simulated tube is essentially composed of iron with an outer diameter of 280 mm and 10 mm thickness. It includes a barium sulfate scale ($BaSO_4$) of varying thickness and crude oil as fluid. The simulated configuration is shown in Fig. 1 and was based on previous studies (Salgado et al., 2010; Salgado et al., 2019; Oliveira et al., 2015; Teixeira et al., 2018).

A 3D view of the simulated system is shown in Fig. 2.

The simulations consisted of 1301 different maximum thicknesses for each location of scale within the pipeline. The maximum scale locations are where most of the barium sulfate deposition is located, with the greatest thickness of deposition. Therefore, the incrustations were simulated in four different locations, in relation to the point source, inside the pipe, at 0°, 30°, 60° and 90°, as shown in Fig. 3.

The thickness of the scale for each position ranged from 5 mm (minimum thickness) to 135 mm (maximum thickness, depicting an extreme case of deposition) with1mm steps, totaling 5204 different thicknesses and simulated positions. The $BaSO_4$ scale deposition considered in this study was an eccentric ring geometry. The liquid phase used was crude oil with a density of 0.973 g cm^{-3}.

To obtain the simulation data, one of the output commands available in code MCNPX was used. To calculate the PHD obtained at the detector (MeV) and to study the scale thicknesses, the F8 command (tally card) was used. These commands present a relative error due to the counts in each spectrum energy range. The number of stories (NPS) used was determined to obtain acceptable statistics, with relative error values of less than 5% for 662 keV, according to the MCNPX manual (Pelowitz, 2005).

2.2. Material's linear attenuation coefficient

When a gamma or X-ray beam strikes a material of thickness x, part of the beam is scattered, part is absorbed by the processes already described and a fraction passes through the material without interacting. Emerging beam intensity I is associated with incident beam intensity I_o, by Eq. (1):

$$\frac{I}{I_o} = e^{-\mu x} \tag{1}$$

where:

μ is the probability of the beam "undergoing" attenuation due to Compton scattering, photoelectric absorption or pairing events, being called the Total Linear Attenuation Coefficient.

The linear attenuation coefficient for barium sulfate scale, pipeline and oil is determined by transmission of a monoenergetic pencil-beam beam by means of the Beer-Lambert equation according to Eq. 2

$$\frac{I}{I_o} = e^{-(\mu P * xP \; + \; \mu F * xF \; + \; \mu S * xS)} \tag{2}$$

where:

I: intensity of un-collided photons ($\gamma.cm^{-2}.\ s^{-1}$);
I_o: intensity of primary photons ($\gamma.cm^{-2}.\ s^{-1}$);
μ: linear attenuation coefficient (cm^{-1});
x: beam path length through the absorber (cm);
P - pipeline, F - fluid e S – scale;

The density and thickness of the absorbers are essential for the DNN training, since the linear attenuation coefficient depends on these two parameters to obtain the scale thickness. The linear attenuation coefficients for all materials used in this study were calculated using a very collimated point source (pencil-beam), a surface detector and the desired material (iron tube, barium sulfate scale and oil) in the middle. The linear attenuation coefficient was calculated by Eq. (1) and required density ($g.cm^{-3}$) and mass fraction of the materials, based on their composition, were used as input data for the MCNPX code. The mass attenuation coefficient ($cm^2.g^{-1}$) was theoretically validated using data from the National Institute of Standards and Technology (NIST Standard Reference Database 126, 2004).

2.3. Compton effect (or Incoherent scatter)

In the Compton effect, the photon incident is scattered by a low-binding electron, which receives only part of its energy, continuing its survival within the material in another direction and with less energy. Since the energy transfer depends on the direction of the emerging electron and it is random, a fixed energy photon can result in electrons with variable energy ranging from zero to a maximum value (Knoll, 1989).

Thus, the information associated with the emerging electron is uninteresting from the point of view of detecting incident photon energy. Its distribution in the counting spectrum is random, approximately rectangular. The scattered photon energy E'γ depends on the incident photon energy Eγ and the scattering angle θ in relation to the incident photon direction given by Eq. (3). The probability of this phenomenon occurring is directly proportional to the photon energy and inversely to the atomic number of the target.

$$E^{'}\gamma = \frac{hv}{1 + \frac{hv}{m_o \ c^2}(1 - cos\theta)} \tag{3}$$

where:

hv: Incident photon energy (eV);
m_oc^2 : Electron resting energy (eV);
θ : Scatter angle.

The detectors with the contribution of the scattered beams were essential for the study carried out in this study. The non-uniformity of deposition of eccentric scales makes it impossible to use only one transmission detector. Assuming that the location of maximum deposition is unknown, the detection of scattering in other points around the pipeline was essential to compose the necessary data for training and convergence of the DNN.

2.4. The DNN model

The ANNs are mathematical models, conceptually inspired by the functioning of the brain, which main feature is the ability to learn by example, discovering behaviours and patterns from raw data (a finite set of information). In addition, the ANNs are able to generalize the knowledge acquired during the training process and respond adequately to new situations, not included in the training set (Haykin, 1999). The ANNs have been shown to be easy to apply and efficient, especially in problems where there is no analytical formulation or where prior knowledge of the distribution of variables is not required, or when the problem itself constantly changes over time. The functioning of an ANN can be described in two distinct phases: the training phase (offline phase) is performed by the use of a learning algorithm, where ANN must learn the patterns of a finite set of previously provided examples; the operating phase (online phase) in which ANN is used to respond to new situations.

In their learning process, the ANNs use an approach based on layers of learning (hierarchical learning) to extract the representation of the knowledge present in the raw data. Thus, the ANNs are composed of connected layers of non-linear processing units, called neurons. Starting

from the input layer, that receives the input signal (raw data), each successive internal layer of neurons (usually called hidden layer) transforms the signal, and with enough transformations, the network can learn to represent the complex non-linear relationships of the input (Schmidhuber, 2015; LeCun et al., 2015; Benuwa et al., 2016). Furthermore, the number of hidden layers and neurons is important parameter to define the learn capacity of an ANN. Since the number of hidden layers defines the quantity of parameterized transformations an input signal encounters as it propagates from the input layer to the output layer. In this context, Deep Neural Networks (DNNs) which are ANNs architectures with many hidden layers are able to represent and learn complex functions far more efficiently than Shallow Neural Networks (SNNs), ANNs architectures with few hidden layers (Srivastava et al., 2015).

Considering the nature of the problem of scale thickness and location prediction tackled in this study, it was searched a DNN model fitted to solve supervised learning tasks (input/output learning) and proficient in interpolation and prediction. Moreover, other aspect which was considered for the choosing of the model was its capability to be efficiently trained. Since, the training process of the DNNs is more complex than of the SNNs, due to the many hidden layers of neurons that compose the DNNs and consequently the greater number of parameterized transformations that an input signal encounters as it propagates per the network.

In this sense, one of the main aspects of a DNN is the non-linear and differentiable activation function utilized to activate the neurons of the hidden layers. Since it is this function that dictates the non-linear transformation of the input signal. For a long time, the sigmoid functions (as the logistic sigmoid) were the most popular ANN activation functions option. However, DNN models with more than 4 hidden layers whose implement sigmoid functions tend to present a poor performance, converging more slowly and apparently towards ultimately poorer local minima (Glorot and Bengio, 2010). For this reason (Glorot et al., 2011), proposed a novel DNN architecture that replaces the traditional sigmoid functions utilized to activate the neurons of the hidden layers of the network for rectified functions, due to this the name of this type of DNN model is Deep Rectifier Neural Network (DRNNs). Comparative studies conducted by Glorot et., al demonstrated that DRNNs have better training and generalization capability than sigmoid activated DNNs. The results achieved were considered by the authors a new milestone in the performance of DNNs when applied to supervised learning problems. Along these lines, more recent works (Pedamonti, 2018, Santos et., al 2019, Desterro et., 2020, Pinheiro et al., 2020) ratify the results of Glorot et al. showing that DRNNs are able to achieve higher prediction precision and a lower error rate than the DNNs activated with a sigmoid function in different supervising learning tasks.

Taking the aspects discussed in consideration, in this study, the DRNN was the DNN models selected to tackle the task of predict the scale thickness.

2.5. The simulated data

The data samples are a fundamental part of this work since these are used for the DRNNs training and testing. Therefore, in order to supply a DRNN with a proper amount of training samples, a total of 5204 simulations were performed, 1301 different maximum thicknesses for each location of scale within the pipeline. The maximum thickness of the eccentric scale was evaluated with the aid of three detectors distributed orthogonally around the pipe. Four different positions of the maximum scale within the pipe were studied. By adopting a cartesian plane for the pipe-scale-fluid system, which has symmetry between the quadrants, the displacement of the positions of the mentioned thicknesses would be sufficient to obtain measurements throughout the pipe.

Through the simulations a dataset with 5204 samples, corresponding to 1301 samples of different eccentric scale thicknesses for each of the four different positions within the pipe, was formed. The samples in the dataset have the following input/output structure:

Input Data:

- Detector 1: 662 keV energy counts (137Cs - Channel 67) recorded by detectors in simulations with the geometry defined in MCNPX code, PHD with 10 keV per channel;
- Detector 2 and 3: Energy counts from 20 to 670 keV (C20, C30, …, C670) recorded by detectors 2 and 3 in simulations with geometry defined in code MCNPX, PHD with 10 keV per channel.

Output Data:

- Maximum scale thicknesses, ranging in thickness from 5 mm to 135 mm in 1 mm steps;
- Location of the scale.

2.6. The DRNN design

One of the main drawbacks and challenges in the utilization of backpropagation neural networks, as the DRNNs, is the proper determination of its hyperparameters which are the parameters that are defined before training, for instance the number of neurons and layers. Usually, the hyperparameters are manually defined using a trial and error approach guided by knowledge of a specialist, however, this manual strategy is tedious and often impractical. Therefore, in the last years, some automated approaches for solving this problem have been studied in the literature. Some automated methods that can be cited: Random Search (Bergstra and Bengio, 2012); Robust Design of Artificial Neural Networks (RDANN) (Ortiz-Rodríguez, et., al 2013); Bayesian Optimization (Snoek et., al 2012; Dewancker et., al 2015; Shahriari et., al 2016).

In this sense, in this work, an automated method was used to help the design process of a DRNN model for the scale thickness and location prediction task. For this, a Bayesian optimization method was implemented using the python hyperparameter optimization library Hyperas (Pumperla, 2017).

Using this approach, the following set of hyperparameters and their ranges were defined for the search process:

- Number of Hidden Layers: from 1 to 10 with step of 1;
- Number of Neurons in the Hidden Layers: from 100 to 1000 with step of 100;
- Hidden Layers Activation Function: ReLu (Glorot and Bengio, 2010) or Elu (Clevert et al., 2015;
- Batch Size: from 32 to 128 with step of 32;
- Optimizer: Stochastic Gradient Descendent (SGD), RMSprop (Tieleman and Hinton, 2012) or Adam (Kingma and Ba, 2014)].

On the other hand, the following hyperparameters were manually set.

- Number of Epochs: 1000;
- Error Function: Mean Squared Error.

In addition, in order to perform this hyperparemeters search, the original dataset with 5204 was divided in two sets:

- Training set: Consisting of 80% of the original dataset, containing 4163 samples (1040 for position 60 and 1041 for positions 0, 30, 90);
- Test set: Consisting of 20% of the original dataset, containing 1041 samples (261 for position 60 and 260 for positions 0, 30, 90).

Further, before the training, with the objective of improve the efficiency of the DRNNs models, the input data in these sets were normalized according to Eq. (4).

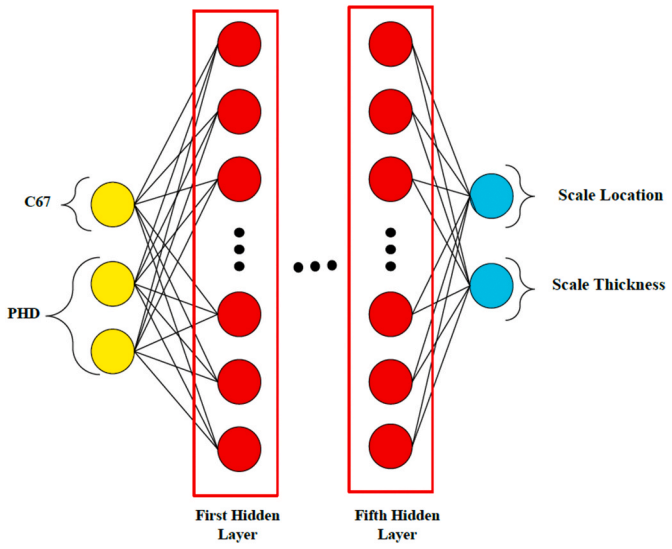

Fig. 4. DRNN architecture proposed for prediction of thickness and location of scale.

Table 1
Comparison of the mass attenuation coefficient for the different materials obtained using the MCNPX code and compared with NIST.

Data	Iron	Barium Sulfate	Atmospheric air	Crude oil
Density	7.874	4.5	1.21E-03	0.896
μ: MCNPX ($cm^2.g^{-1}$)	5.78E-01	1.90E-01	9.30E-05	8.77E-02
μ: NIST ($cm^2.g^{-1}$)	5.80E-01	1.96E-01	9.49E-05	8.88E-02
Relative error (%)	0.29	3.12	1.97	0.41

$$X_N = \frac{(X - X')}{S} \quad (4)$$

where: X_N is the normalized value; X is the original value; X' is the average and S is the standard deviation.

The DRNN that achieved the best result (the smallest mean squared error in the test set) in this automated hyperparameters search has the following characteristics:

- Number of Hidden Layers: 5
- Number of Neurons in the Hidden Layers: [700, 800, 300, 600, 800]
- Hidden Layers Activation Function: ReLu
- Batch Size: 32
- Optimizer: Adam

Fig. 4 illustrates this DRNN architecture.

2.7. The DRNN validation

In order validate the performance of the DRNN model, the K-Fold cross-validation technique was implemented. This technique randomly divides a dataset into K disjoint groups (folds) with approximately equal size, and each fold is in turn used to test of the model induced from the other K-1 folds (Wong, 2015).

The implementation of the K-Fold in this study can be summarized as follows:

1. The original dataset (with samples already normalized) was divided 10 folds (K = 10), with each fold corresponding to 20% of the original dataset size;
2. For 10 times, one of the 10 folds was used as test set to evaluate the performance of the DRNN model and the other K - 1 folds were grouped to form a training set to train the DRNN;
3. At end of the process, the average error for the 10 experiments were computed.

3. Results

The mass attenuation coefficient (μ/ρ) obtained by MCNPX code, calculated using Eq. (1), was compared with the NIST data and the result

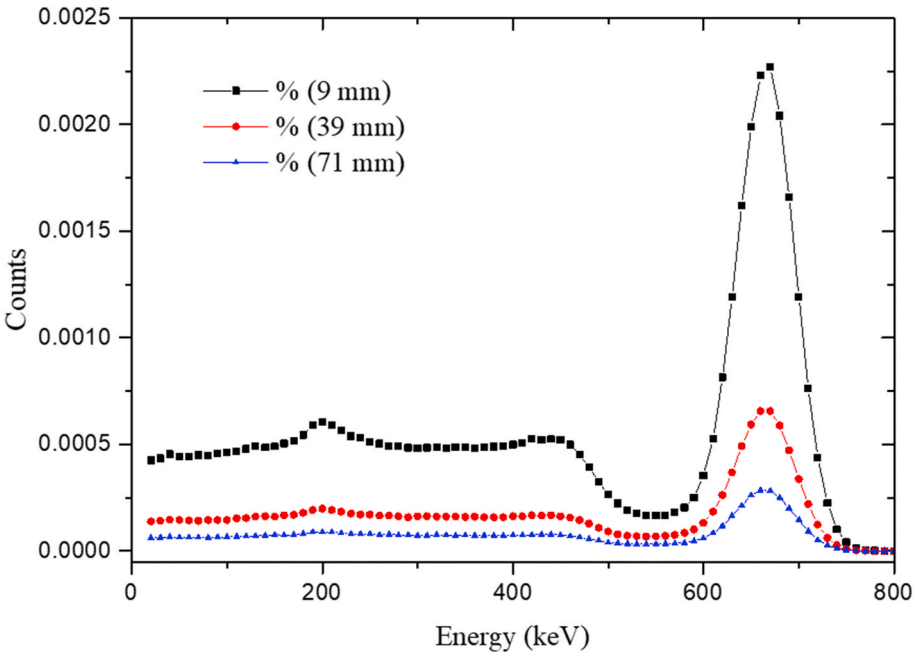

Fig. 5. PHD for different eccentric thickness of scale for beam transmitted.

Table 2
DRNN performance in the K-Fold cross-validation.

	Scale Thickness Prediction Metrics										Scale Position Prediction Metric	
	MAE		MSE		RMSE		MARE		R2 Score		Accuracy	
	Train	Test	Train	Test	Train	Test	Train	Test	Train	Test	Train	Test
1	0.01650	0.01749	0.00159	0.00176	0.03994	0.04194	0.26723%	0.28868%	0.9998873	0.9998735	100%	100%
2	0.01727	0.01668	0.00165	0.00141	0.04065	0.03752	0.30672%	0.31830%	0.9998831	0.9998991	100%	100%
3	0.01728	0.01725	0.00163	0.00179	0.04038	0.04230	0.35294%	0.33352%	0.9998839	0.9998750	100%	100%
4	0.01697	0.01752	0.00161	0.00200	0.04012	0.04468	0.28384%	0.29008%	0.9998858	0.9998591	100%	100%
5	0.01647	0.01850	0.00158	0.00199	0.03970	0.04466	0.28145%	0.31236%	0.9998876	0.9998617	100%	100%
6	0.01697	0.01672	0.00175	0.00136	0.04180	0.03692	0.26913%	0.25806%	0.9998763	0.9999026	100%	100%
7	0.01644	0.01650	0.00165	0.00141	0.04061	0.03754	0.26381%	0.27662%	0.9998840	0.9998970	100%	100%
8	0.01633	0.01693	0.00155	0.00181	0.03935	0.04255	0.26343%	0.27813%	0.9998901	0.9998722	100%	100%
9	0.01753	0.01882	0.00161	0.00204	0.04011	0.04521	0.30641%	0.31857%	0.9998846	0.9998614	100%	100%
10	0.01636	0.01696	0.00161	0.00128	0.04017	0.03580	0.26545%	0.30596%	0.9998853	0.9999118	100%	100%
Average	**0.01681**	**0.01734**	**0.00162**	**0.00169**	**0.04028**	**0.04091**	**0.28604%**	**0.29803%**	**0.9998848**	**0.9998813**	**100%**	**100%**

*MAE - Mean Absolute Error; MSE - Mean Squared Error; RMSE - Root Mean Squared Error; MARE - Mean Absolute Relative Error.

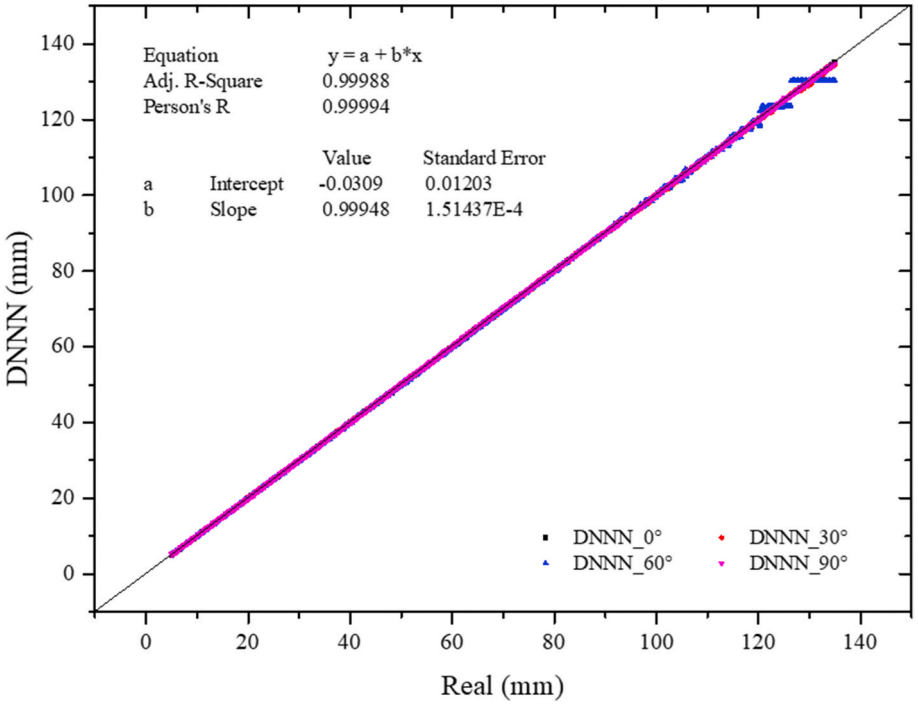

Fig. 6. Correlations of eccentric scale thickness by MCNPX code and obtained by DRNN for all standards.

is shown in Table 1. These values were used to calculate the thickness of the scale under different positions.

Comparisons between mass attenuation coefficients show a relative error of less than 3.2%, indicating that the models developed at MCNPX code can be used for reliable DRNN training.

In Fig. 5 is the expected spectrum for three different scale thicknesses. It is worth mentioning that the X-ray of the K shell of $^{137m}Ba_{56}$ ($BaK\alpha_1$) was not considered in the simulation because it plays no role in the process.

Table 2 shows the performance of the DRNN model using the K-Fold cross validation method.

The metrics in Table 2 shows that for the 10 experiments realized using the cross validation approach the DRNN was able to achieve satisfactory results both in the training set and test set. Taking into the account that each test set have 1041 samples of untrained scales thickness in different locations, the average values (MAE = 0.01734, MSE = 0.00169, RMSE = 0.04091, MARE = 0.29803% and R2 Score = 0.9998813) show that the model has good generalization capability, meaning that the DRNN is able to predict the maximum incrustation thickness for untrained samples with very small errors. Besides that, since in all experiments the model predicted the scale position with 100% of accuracy, it can be stated that the DRNN is able to adequately predict the thickness of the eccentric scale regardless of its location is inside the pipe.

Considering individually the R2 Score value, the experiment 4 was the one where the DRNN demonstrated the worst performance for this

Table 3
Percentage of predictions of experiment four distributed in ranges of absolute relative errors.

Percentage of Samples	Absolute Relative Error Range
92.8846%	<1%
4.8076%	1%–2%
1.8269%	2%–3%
0.3846%	3%–4%
0.0961%	>4%

metric. Therefore, this particular experiment will be more deeply analyzed. In this context, Fig. 6 shows the values predicted by the DRNN in comparison with the data considered in the simulations.

The eccentric scale data predicted by the DRNN were adjusted to a linear equation by the method of least squares. While, Table 3, presents the percentage of predictions of experiment four distributed in ranges of absolute relative errors.

The results in Fig. 6 and Table 3 show that the DRNN even in its worst performance scenario is still able to achieve good generalization capacity.

4. Conclusions

The objective of this study is to determine the thickness of scaling with eccentric deposition regardless of its location. The approach adopted was based on the recognition of PHD patterns obtained by three scintillating detectors from a trained and validated deep artificial neural network (DNN) model, more specifically a 7-layers deep rectifier neural network (DRNN), with data generated by simulated models based on the Monte Carlo method, MCNPX code. The 7-layers DRNN model utilized was designed using a Bayesian optimization method via the library Hyperas, while the validation of this model performance was verified using the K-Fold cross validation method. Using the crossvalidation methodology 10 experiments were realized, in each, different randomly distribution of eccentric scale thickness samples was utilized to form the training and test set, which are used respectively, to train and test the generalization capability of the model. The DRNN for test sets was able to achieve an average MAE of 0.01734, MSE of 0.00169, RMSE of 0.04091, MARE of 0.29803% and R2 Score = 0.9998813 for the scale thickness prediction and an average accuracy of 100% for the scale position. These results show that the DRNN has a good generalization capability, being able to predict the maximum incrustation thickness for untrained samples with very small errors, regardless of its location is inside the pipe. Therefore, it can be inferred that the proposed methodology for calculating scale formed by barium sulfate ($BaSO_4$) by the DRNN is a promising and suitable technique to solve this type of problem, especially in cases where it is not possible to obtain internal information. In the proposed approach, it is important to note that no prior knowledge about the presence of fluids and fractions is required if the neural network is properly trained. The pipe-scale-fluid system is also capable of predicting scale thickness with just one measurement, providing less time for data acquisition and processing and therefore faster identification of deposition, demonstrating high applicability in the industry.

Acknowledgments

The authors would like to acknowledge: the National Council for Scientific and Technological Development (CNPq) and Petrobras for financial support. The Alberto Luiz Coimbra Institute for Graduate Studies and Research in Engineering (COPPE) and Nuclear Engineering Institute (IEN) for academic support.

References

Abdul Majid, S., 2013. Determination of wax deposition and corrosion in pipelines by nêutron back diffusion collimation and neutron capture gamma-rays. Appl. Radiat. Isot. 74, 102–108. https://doi.org/10.1016/j.apradiso.2013.01.012.

Abdul-Majid, S., Dawood, O., 1989. Neutron-capture gamma ray technique for scale identification inside pipes. Desalination 75, 199–210. https://doi.org/10.1016/0011-9164(89)85014-3, 1989.

Abdul-Majid, S., Melaibari, A., Malki, B., 1996. Hydrocarbon scale deposit measurements by neutron moderation and capture gamma method. Nucl. Instrum. Methods Phys. Res. B 119, 433–437. https://doi.org/10.1016/0168-583X(96)00296-0, 1996.

Abro, E., Khoryakov, V.A., Johansen, G.A., Kocbach, L., 1999. Determination of void fraction and flow regime using a neural network trained on simulated data based on gamma-ray densitometry. Meas. Sci. Technol. 10, 619–630. https://doi.org/10.1088/0957-0233/10/7/308.

Achmad, B., Hussein, E.M.A., 2004. An X-ray Compton scatter method for density measurement at a point within an object. Appl. Radiat. Isot. 60, 805–814. https://doi.org/10.1016/j.apradiso.2003.12.005.

Amiri, M., Moghadasi, J., 2010. Prediction the amount of Barium Sulfate scale formation in Siri oilfield using OLI ScaleChem software. Asian J. Sci. Res. 3, 230–239. https://doi.org/10.3923/ajsr.2010.230.239.

Araújo, A.A., 2005. Radiochemical determination of ^{210}Pb e ^{226}Ra in sludge and oil scale. M.S. thesis. Universidade Federal de Pernambuco, Recife, PE, Brasil (in portuguese).

Benuwa, B.B., Zhan, Y.Z., Ghansah, B., Wornyo, D.K., Banaseka Kataka, F., 2016. A review of deep machine learning". Int. J. Eng. Res. Afr. 24, 124–136. https://doi.org/10.4028/www.scientific.net/JERA.24.124.

Bergstra, J., Bengio, Y., 2012. Random search for hyper-parameter optimization. J. Mach. Learn. Res. 13, 281–305.

Berman, A.I., Harris, J.N., 1954. Precision measurement of uniformity of materials by gamma-ray transmission. Rev. Sci. Instrum. 25 (1), 21–29. https://doi.org/10.1063/1.1770876.

Beserra, M.T.F., 2012. Scale Thickness Evaluation in Oil Extraction Ducts. Master Thesis, Instituto de Radioproteção e Dosimetria, Rio de Janeiro, RJ, Brasil (in Portuguese).

Bjørnstad, T., Stamatakis, E., 2006a. Scaling studies with gamma transmission technique. Oilfield Chem. 19–22. Geilo, NORWAY.

Bjørnstad, T., Stamatakis, E., 2006b. Applicability and Sensitivity of Gamma Transmission and Radiotracer Techniques for Mineral Scaling Studies. Institute for Mineral Scaling Studies, Institute for Energy Technology, NORWAY.

Bukuaghangin, O., Sanni, O., Kapur, N., Huggan, M., Neville, A., Charpentier, T., 2016. Kinetics study of barium sulfate surface scaling and inhibition with aonce-through flow system. J. Petrol. Sci. Eng. 147, 699–706. https://doi.org/10.1016/j.petrol.2016.09.035.

Candeias, J.P., Oliveira, D. F. de, Anjos, M. J. dos, Lopes, R.T., 2014. Scale analysis using X-ray microfluorescence and computed radiography. Radiat. Phys. Chem. 95, 408–411. https://doi.org/10.1016/j.radphyschem.2013.03.007. February 2014.

Clevert, D.A., Unterthiner, T., Hochreiter, S., 2015. Fast and Accurate Deep Network Learning by Exponential Linear Units (Elus) arXiv preprint arXiv:1511.07289.

Coto, B., Martos, C., Peña, J.L., Espada, J.J., Robustillo, M.D., 2008. A new method for determination of wax precipitation from non-diluted oils by fractional precipitation. Fuel 87, 2090–2094. https://doi.org/10.1016/j.fuel.2007.12.012.

Desterro, F.S.M., Santos, M.C., Gomes, K.J., Heimlich, A., Schirru, R., Pereira, C.M.N.A., 2020. Development of a Deep Rectifier Neural Network for dose prediction in nuclear emergencies with radioactive material releases. Prog. Nucl. Energy 118. https://doi.org/10.1016/j.pnucene.2019.103110.

Dewancker, I., McCourt, M., Clark, S., 2015. Bayesian Optimization for Machine Learning: A Practical Guidebook. SigOpt, San Francisco, CA 94108 arXiv: 1612.04858.

Drake, S.G., Seward, J.C., 1989. "Radiographic Detection of Pipe Corrosion under Lagging". GB2211708A. UK Patent Application, UK.

Ferreira, V.F., Reis, M.I.P., Silva, F.C., Romeiro, G.A., Rocha, A.A., 2011. Mineral deposition on surfaces: problems and opportunities in the oil industry. Revista Virtual de Química 3, 2–13. https://doi.org/10.5935/1984-6835.20110002 (in Portuguese).

Gheisari, M., Wang, G., Bhuiyan, M.Z.A., 2017. A survey on deep learning in big data. In: 2017 IEEE International Conference on Computational Science and Engineering (CSE) and IEEE International Conference on Embedded and Ubiquitous Computing. EUC), Guangzhou, pp. 173–180.

Glorot, X., Bengio, Y., 2010. Understanding the difficulty of training deep feedforward neural networks. Proc. AISTATS 9, 249–256.

Glorot, X., Bordes, A., Bengio, Y., 2011. Deep sparse rectifier neural networks. Proceedings of the fourteenth international conference on artificial intelligence and statistics. PMLR 15, 315–323.

Godoy, J.M., Cruz, R.P., 2003. ^{226}Ra and ^{228}Ra in scale and sluge samples and their correlation with the chemical composition. J. Environ. Radioact. 70, 199–206. https://doi.org/10.1016/S0265-931X(03)00104-8.

Graham, A.L., Vieille, E., Neville, A., Boak, L.S., Sorbie, K.S., 2004. Inhibition of BaSO4 at a Hastelloy Metal Surface and in Solution: the Consequences of Falling below the Minimum Inhibitor Concentration (MIC). Society of Petroleum Engineers. https://doi.org/10.2118/87444-MS.

Haykin, S., 1999. Neural Networks, second ed. A Compreensive Foundation, Prentice-Hall, Hamilton, Ontario, Canada.

Kan, A., Tomson, M., 2012. Scale prediction for oil and gas production, 17. Society of Petroleum Engineers Journal, p. 332. https://doi.org/10.2118/132237-PA.

Khatami, H.R., Ranjbar, M., Schaffie, M., Emady, M.A., 2010. Development of a fuzzy saturation index for sulfate scale prediction. J. Petrol. Sci. Eng. 71, 13–18. https://doi.org/10.1016/j.petrol.2009.12.006.

Kingma, D., Ba, Jimmy, 2014. Adam: A Method for Stochastic Optimization arXiv preprint arXiv:1412.6980.

Knoll, G.F., 1989. Radiation Detection and Measurement, second ed. John Wiley & Sons, Inc., pp. 51–52

LeCun, Y., Bengio, Y., Hinton, G., 2015. Deep learning. Nature 521, 436–444.

Lewis, J.W., Van Essen, D.C., 2000. Mapping of architectonic subdivisions in the macaque monkey, with emphasis on parieto-occipital cortex. J. Comp. Neurol. 428 (1), 79–111.

Martin, A., Mead, S., Wade, B.O., 1997. Materials, Containing Natural Radionuclides in Enhanced Concentrations. European Commission Report, Catalogue Number: CRNA 17625 ENC.

Mi, Y., Ishii, M. E, Tsoukalas, L.H., "Vertical two-phase flow identification using advanced instrumentation and neural networks". Nucl. Eng. Des., vol. 184, pp. 409-420. https://doi.org/10.1016/S0029-5493(98)00212-X.

Monno, A., 1985. "Tube wall thickness" GB patent document 2146115/A/, GB patent application 8323913. Int. Classif. G01B 15/02, 9. April.
NIST Standard Reference Database 126, 2004. https://dx.doi.org/10.18434/T4D01F. (Accessed 15 August 2018).
Olajire, A.A., 2015. A review of oilfield scale management technology for oil and gas production. J. Petrol. Sci. Eng. 135, 723–737. https://doi.org/10.1016/j.petrol.2015.09.011.
Oliveira, D.F., Nascimento, J.R., Marinho, C.A., Lopes, R.T., 2015. Gamma transmission system for detection of scale in oil exploration pipelines. Nucl. Instrum. Methods Phys. Res., Sect. A 784, 616–620. https://doi.org/10.1016/j.nima.2014.11.030.
Oliveira, D.F., Santos, R.S., Machado, A.S., Silva, A.S.S., Anjos, M.J., Lopes, R.T., 2019. Characterization of scale deposition in oil pipelines through X-Ray Microfluorescence and X-Ray microtomography. Appl. Radiat. Isot. 151, 247–255. https://doi.org/10.1016/j.apradiso.2019.06.019.
Ortiz-Rodriguez, J.M., Martinez-Blanco, M.R., Varamontes, Vega-Carrillo, J.M., R, H., 2013. In: Suzuki, K. (Ed.), Robust Design of Artificial Neural Networks Methodology in Neutron Spectrometry. Artificial Neural Networks - Architectures and Applications.
Pedamonti, D., 2018. Comparison of Non-linear Activation Functions for Deep Neural Networks on MNIST Classification Task. CoRR - Computing Research Repository.
Pelowitz, D.B., 2005. "MCNPX TM User's Manual" Version 2.5.0, LA-CP-05-0369. Los Alamos National Laboratory.
Pinheiro, V.H.C., Santos, M.C., Desterro, F.S.M., Schirru, R., Pereira, C.M.N.A., 2020. Nuclear Power Plant accident identification system with "don't know" response capability: novel deep learning-based approaches. Ann. Nucl. Energy 137. https://doi.org/10.1016/j.anucene.2019.107111.
Pumperla, M., 2017. Hyperas: a very simple convenience wrapper around hyperopt for fast prototyping with keras models. https://maxpumperla.com/hyperas/. (Accessed 27 March 2020).
Roshani, G.H., Feghhi, S.A.H., Adineh-Vand, A., Khorsandi, M., 2013. Application of adaptive neuro-fuzzy inference system in prediction of fluid density for a gamma-ray densitometer in petroleum products monitoring. Measurement 46, 3276–3281. https://doi.org/10.1016/j.measurement.2013.07.005.
Roshani, G.H., Nazemi, E., Feghhi, S.A.H., 2015. Flow regime identification and void fraction prediction in two-phase flows based on gamma ray attenuation. Measurement 62, 25–32. https://doi.org/10.1016/j.measurement.2014.11.006.
Roshani, G.H., Nazemi, E., Roshani, M.M., 2017a. A novel method for flow pattern identification in unstable operational conditions using gamma ray and radial basis function. Appl. Radiat. Isot. 123, 60–68. https://doi.org/10.1016/j.apradiso.2017.02.023.
Roshani, G.H., Karami, A., Salehizadeh, A., Nazemi, E., 2017b. The capability of radial basis function to forecast the volume fractions of the annular three-phase flow of gas-oil-water. Appl. Radiat. Isot. 129, 156–162. https://doi.org/10.1016/j.apradiso.2017.08.027.
Roshani, G.H., Karami, A., Khazaei, A., Olfateh, A., Nazemi, E., Omidi, M., 2018. Optimization of radioactive sources to achieve the highest precision in three-phase flow meters using Jaya algorithm. Appl. Radiat. Isot. 139, 256–265. https://doi.org/10.1016/j.apradiso.2018.05.015.
Salgado, C.M., Brandão, L.E.B., Schirru, R., Pereira, C.M.N.A., Silva, A.X., Ramos, R., 2009. Prediction of volume fractions in three-phase flows using nuclear technique and artificial neural network. Appl. Radiat. Isot. 67, 1812–1818. https://doi.org/10.1016/j.apradiso.2009.02.093.
Salgado, C.M., Pereira, C.M.N.A., Schirru, R., Brandão, L.E.B., 2010. Flow regime identification and volume fraction prediction in multiphase flows by means of gamma-ray attenuation and artificial neural networks. Prog. Nucl. Energy 52, 555–562. https://doi.org/10.1016/j.pnucene.2010.02.001.
Salgado, W.L., Dam, R.S.F., Teixeira, T.P., Conti, C.C., Salgado, C.M., 2019. Application of artificial intelligence in scale thickness prediction on offshore petroleum using a gamma-ray densitometer. Radiat. Phys. Chem. 168, 108549 https://doi.org/10.1016/j.radphyschem.2019.108549.
Santos, M.C., Pinheiro, V.H.C., Desterro, F.S.M., Avellar, R.K., Schirru, R., Nicolau, A.S., Lima, A.M.M., 2019. Deep rectifier neural network applied to the accident identification problem in a PWR nuclear power plant. Ann. Nucl. Energy 133, 400–408. https://doi.org/10.1016/j.anucene.2019.05.039.
Schmidhuber, J., 2015. Deep learning in neural networks: an overview. Neural Netw. Off. J. Int. Neural Netw. Soc. 61, 85–117.
Shahriari, B., Swersky, K., Wang, Z., Adams, R.P., de Freitas, N., 2016. Taking the human out of the loop: a review of bayesian optimization. Proc. IEEE 104 (1), 148–175.
Snoek, J., Larochelle, H., Adams, R., 2012. Practical Bayesian optimization of machine learning algorithms. In: Advances in Neural Information Processing Systems, vol. 25, pp. 2960–2968, 2012.
Sowerby, B.D., Rogers, C.A., 2005. Gamma-ray density and thickness gauges using ultra-low activity radioisotope sourcefillin. Appl. Radiat. Isot. 63, 789–793. https://doi.org/10.1016/j.apradiso.2005.05.031, 2005.
Srivastava, R.K., Greff, K., Schmidhuber, J., 2015. Training very deep networks. In: The Swiss AI Lab IDSIA/USI/SUPSI, Neural Information Processing Systems (NIPS).
Teixeira, T.P., Salgado, C.M., 2017. Use of transmission gamma for study of calculation of scale thickness in oil pipelines. INIS 49 (1). INIS issue 7 (1). International Nuclear Atlantic Conference; Belo Horizonte, MG (Brazil).
Teixeira, T.P., Salgado, C.M., Dam, R.S.F., Salgado, W.L., 2018. Inorganic scale thickness prediction in oil pipelines by gamma-ray attenuation and artificial neural network. Appl. Radiat. Isot. 141, 44–50. https://doi.org/10.1016/j.apradiso.2018.08.008.
Tieleman, T., Hinton, G., 2012. Lecture 6.5-rmsprop: divide the gradient by a running average of its recent magnitude. COURSERA: Neural Netw. Mach. Learn. 4 (2).
Wong, T.-T., 2015. Performance evaluation of classification algorithms by k-fold and leave-one-out cross validation. Pattern Recogn. 48 (9), 2839–2846. https://doi.org/10.1016/j.patcog.2015.03.009.
Yan, F.Y., Dai, Z., Ruan, G., Alsaiari, H., Bhandari, N., Zhang, F., Liu, Y., Zhang, Z., Kan, A., Tomson, M., 2004. Barite scale formation and inhibition in laminar and turbulent flow: a rotating cylinder approach. J. Petrol. Sci. Eng. 149, 183–192. https://doi.org/10.1016/j.petrol.2016.10.030.